Schepers, A., Milsch, H. (2013): Relationships between fluid-rock interactions and the electrical conductivity of sandstones. - Journal of Geophysical Research, 118, 7, 3304-3317

DOI: 10.1002/jgrb.50241

Relationships Between Fluid-Rock Interactions and the Electrical Conductivity of Sandstones

A. Schepers[1] and H. Milsch[1]

A. Schepers, Helmholtz Centre Potsdam, GFZ German Research Centre for Geosciences, Telegrafenberg, 14473 Potsdam, Germany, (ansgar.schepers@gmail.com)

H. Milsch, Helmholtz Centre Potsdam, GFZ German Research Centre for Geosciences, Telegrafenberg, 14473 Potsdam, Germany, (harald.milsch@gfz-potsdam.de)

[1]Helmholtz Centre Potsdam, GFZ
German Research Centre for Geosciences,
Telegrafenberg, 14473 Potsdam, Germany.

Abstract. Batch and flow-through experiments were performed on quartz-feldspar granular aggregates and sandstone samples to investigate time-dependent effects of fluid-rock interactions on fluid and rock conductivity, respectively. The experiments were conducted at temperatures up to 164 °C, at confining and pore pressures up to 10 and 5 MPa, respectively, and for up to 136 days. It showed that changes in rock conductivity were unequivocally related to changes in pore fluid conductivity. It is inferred that these changes were dependent on kinetically controlled dissolution reactions between the mineral grains and the fluid. The time-dependent signature of rock conductivity implied a detectable transition from initial dissolution towards some state of equilibrium. The response of rock conductivity to temperature changes followed an Arrhenius-type behavior. An exploratory kinetic evaluation of the conductivity data for sandstone samples yielded an apparent activation energy E_a^* of approximately 32 kJ/mol. A concurrent chemical fluid analysis showed that this is an integrated value over all reactions occurring in parallel within a sample. These reactions namely concern silica and silicate dissolution but also the dissolution of accessory salt minerals. It is concluded that measuring the evolution of rock conductivity in combination with chemical pore fluid analysis constitutes a powerful and quantitative tool for monitoring time-dependent changes in pore fluid chemistry and thus fluid-rock interactions in real time.

1. Introduction

The electrical conductivity of rocks, σ_r is a widely used parameter in geophysical investigations including oil reservoir assessment, monitoring of hydrothermal fluid flow associated with volcanic activity, prospecting for geothermal resources with magnetotellurics, as well as characterization of the structure and composition the Earth's crust [e.g., *Bussian*, 1983; *Flóvenz et al.*, 1985; *Chelidze and Guéguen*, 1999; *Revil et al.*, 2002; *Yang et al.*, 2011]. Factors controlling changes of σ_r of a porous rock are changes in temperature, saturation of the pore space with an electrically conducting fluid, and concentration of dissolved ionic species, c_i, in the fluid [*Rein et al.*, 2004; *Hayley et al.*, 2007]. The correct interpretation of field surveys of electrical properties requires a sound understanding of the electrical properties of the rocks at the laboratory scale [*Revil et al.*, 2002].

Two parameters contribute to σ_r in a fully saturated porous rock: The electrical conductivity of the pore fluid, σ_f, and the electrical conductivity of mineral-fluid interfaces commonly termed electrical surface conductivity, σ_s. According to Archie's law [*Archie*, 1942] and assuming that the contribution of σ_s to σ_r can be neglected, σ_r is related to σ_f and the porosity ϕ by:

$$\sigma_r = \sigma_f \, \phi^m, \tag{1}$$

where m is the cementation exponent and the formation resistivity factor $F = \phi^{-m}$. Equation 1 has been supplemented to fit results obtained from collections of different sandstone samples:

$$\sigma_r = a^{-1}\,\sigma_f\,\phi^m, \tag{2}$$

where a is an empirical parameter. The range of a and m is constrained by $0.62 < a < 3.5$ and $1.5 < m < 2.5$, where the majority of sandstones exhibits m values close to 2 [*Guéguen and Palciauskas*, 1994; *Regberg et al.*, 2011]. Well-cemented Paleozoic sedimentary rocks with a porosity of 5 to 25 % exhibit $a = 0.62$ and $m = 1.95$ [*Keller*, 1989].

For cases where electrical conductance of the mineral-fluid interfaces contributes significantly to σ_r, Archie's law is expanded by a constant for σ_s assuming a simple model of parallel conductors [*David et al.*, 1993; *Regberg et al.*, 2011]:

$$\sigma_r = a^{-1}\,\phi^m\,\sigma_f + \sigma_s. \tag{3}$$

Empirical models extend Archie's law by empirically derived terms for the contribution of electrical conduction at mineral-fluid interfaces to σ_r [*Waxman and Smits*, 1968; *Sen et al.*, 1988]. Models using the notion of an effective medium describe σ_r as resulting from the presence of volumes with different electrical conductivities, e.g., insulating silicate spheres coated by a conductive clay layer that are immersed in an electrolyte [*Bussian*, 1983; *de Lima and Sharma*, 1990; *Ruffet et al.*, 1995; *Glover et al.*, 2000].

Electrical conductivity of rocks has been frequently investigated as to its relation to σ_f, σ_s, and temperature [e.g., *Waxman and Smits*, 1968; *Roberts and Schwartz*, 1985; *Sen et al.*, 1988; *Sen and Goode*, 1992; *Glover et al.*, 1994; *Nettelblad et al.*, 1995; *Ruffet et al.*, 1995; *Revil and Glover*, 1997; *Revil et al.*, 1998; *Revil and Glover*, 1998; *Roberts et al.*, 2001]. Little data exist on the evolution of σ_r in the course of fluid-rock interactions

[*Piwinskii and Weed*, 1976; *Weed et al.*, 1977; *Kristinsdóttir et al.*, 2010]. Fluid-rock interactions influence c_i and thus σ_f and σ_r.

Batch experiments with various rock types, including graywacke samples consisting of quartz, feldspar, calcite, dolomite and more than 5 % clay minerals in contact with tap-water at room temperature yielded a time-dependent behavior of σ_r and σ_f resulting from cation exchange of the clay minerals and dissolution of other minerals in the rock samples [*Piwinskii and Weed*, 1976; *Weed et al.*, 1977]. Particularly, σ_r first increased with time at a decreasing rate, passed a maximum, and then slightly decreased and approached a constant value. Concurrently, σ_f increased monotonically with time at a decreasing rate. The decreasing rates of σ_r and σ_f resulted from decreasing driving forces for cation exchange and dissolution as c_i increased in the course of the experiments.

Flow-through experiments with altered volcanic rock samples (hyaloclastites and basalts containing different clay minerals) saturated with synthetic geothermal fluids yielded a time-dependent increase of σ_r at decreasing rates at 150 °C and constant confining and pore pressure of up to 28 MPa and 10 MPa, respectively [*Kristinsdóttir et al.*, 2010]. It was concluded that the time-dependent behavior of σ_r at constant p-T-conditions resulted from ion exchange between the clay minerals and the pore fluid.

The aim of the present study was to investigate the effects of fluid-rock interactions on σ_r for clay-bearing sandstones. Batch and flow-through experiments were conducted with clay-bearing sandstones as well as granular materials representing the main mineral phases (quartz and feldspars) of these sandstones. The experiments were conducted at different levels of abstraction of the situation in deep sedimentary reservoirs where the minerals of a sandstone interact with a pore fluid (i.e., a brine). The findings resulting from the

relatively simple batch experiments with quartz-feldspar aggregates and deionized H_2O were used to interpret the results of the more complex systems of clay-bearing sandstones in contact with an evolving pore fluid. Monitoring time-dependent changes of σ_r may be a tool for the assessment of induced dissolution-precipitation reactions both in laboratory investigations of fluid-rock interactions as well as in geotechnical applications such as nuclear waste disposal, CO_2 storage, and geothermal energy production.

2. Experimental Techniques

Two groups of experiments were performed in the present study: (i) Batch experiments were conducted with granular aggregates of quartz, labradorite, and microcline as well as intact samples of Flechtinger sandstone (Table 1) in order to investigate the effects of fluid-mineral reactions on σ_f and c_i. (ii) Flow-through experiments were carried out with sandwiched quartz-feldspar granular aggregates as well as Fontainebleau and Flechtinger sandstone core samples in order to examine the evolution of c_i as well as the concurrent evolutions of σ_f and σ_r under initial disequilibrium conditions. An overview of the batch and flow-through experiments is presented in Table 2.

2.1. Starting Materials and Fluids

The granular aggregates were produced by grinding pegmatitic crystals supplied by Dr. F. Krantz Rheinisches Mineralienkontor, Bonn, Germany as well as Fontainebleau sandstone samples (Table 1) and dry sieving the resulting powder to a grain size smaller than 355 μm. Magnetic particles were removed with a Frantz LB-1 magnetic barrier laboratory separator (current 0.4 A, voltage $\approx$ 23 V). The resulting powders were dry sieved to obtain a grain size fraction of 63 to 125 μm. Larger particles were ground

in an agate pulverizer and dry sieved again. The 63 to 125 μm grain size fraction was ultrasonically cleaned for 1200 s in H_2O and was then wet sieved to obtain two grain size fractions < 63 μm and 63 to 125 μm. X-ray powder diffraction (XRD) analyses and scanning electron microscopic micrographs (SEM) of the powders showed that pure mineral phases of quartz, labradorite, and microcline were obtained by this preparation method. The bulk chemical composition of the granular aggregates was measured with X-ray fluorescence (XRF) and yielded only minor impurities (< 1 %) in the starting materials (Table 3).

The rock samples were a Lower Permian (Upper Rotliegend) sandstone quarried from an outcrop in Flechtingen near Magdeburg, Germany (Flechtinger sandstone), and a quartz sandstone of Oligocene age quarried from an outcrop in the Ile de France region near Paris, France (Fontainebleau sandstone). The mean porosity of the Flechtinger sandstone samples was approximately 10 %. SEM micrographs of the pore space showed that fibrous illite and other cement minerals lined the pore walls and partly filled the pores and the pore throats of the Flechtinger sandstone (Table 1). The porosities of the Fontainebleau sandstone samples were variable due to variations in the cementation. Cylindrical cores with a length of 40 mm and a diameter of 30 mm were produced with orientations parallel and perpendicular to the bedding of macroscopically homogeneous blocks of these sandstones.

The sandwich samples consisted of cylindrical porous discs that sandwiched a granular aggregate of quartz, labradorite, and microcline. In the following, the sandwich samples will be referred to as QLM sandwiches, where Q, L, and M denote quartz, labradorite, and microcline, respectively. The sandwiching porous discs were prepared from porous

polytetrafluoroethylene (PTFE) with a porosity of 20 % as well as from Fontainebleau sandstone samples with approximately 2 % porosity. The length of the sandwich samples ranged between 32 and 40 mm. The diameter of the sandwich samples was 30 mm.

The starting fluid in all but one experiments was deionized H_2O with $\sigma_f(T_0) \approx 2.5$ mS/m at $T_0 = 25$ °C. A 43.2 mmol/L $NaCl_{aq}$ solution with $\sigma_f(T_0) \approx 477$ mS/m was used in one flow-through experiment. The experiment design ensured that the solids were in contact with liquid water even in experiments at high temperatures (up to 164 °C).

2.2. Experiments

Five types of batch and flow-through experiments were performed in the present study: (i) Batch experiments with granular aggregates; (ii) Batch experiments with rock fragments; (iii) A batch experiment with a Flechtinger sandstone sample saturated initially with H_2O; (iv) Flow-through experiments with sandwich samples; (v) Flow-through experiments with rock samples (Figure 1). The types of experiments are described in the following in more detail:

(i) The batch experiments with granular QLM aggregates were conducted in 10 and 20 mL PTFE autoclaves (Bola, Germany). The resulting pressures in the temperature range of 70 to 150 °C ranged between approximately 0.1 and 0.45 MPa. The batch experiments were conducted at constant temperature conditions in a Memmert drying oven. The accuracy of the oven was estimated to be ±2 °C at 70 °C by repeated measurements with an ASL Pt25 reference thermometer. The experiments are labeled b-QLM-3, b-QLM-4, and b-QLM-5 in Table 2.

(ii) The batch experiments with Flechtinger sandstone rock fragments were performed in a 10 mL PTFE autoclave and in a pressurized 0.3 L PTFE lined autoclave with ther-

mal insulation (BR-300, High Preactor, Berghof, Germany). Pressure was maintained at approximately 5 MPa by Ar gas feeding. It is assumed that the influence of dissolved Ar on σ_f was insignificant although a small effect of dissolved nonpolar gases on the molecular water structure has been reported [*Pashley et al.*, 2005]. Temperature was monitored with a type K thermocouple. In this set-up temperatures were stable at 70 ± 2 °C and 150 ± 2 °C. The experiments are labeled b-Fl-15 and b-Fl-16 in Table 2.

(iii) In a third type of batch experiments an H_2O-saturated cylindrical Flechtinger sandstone sample with a length of 100 mm and a radius of 25 mm was jacketed with a FEP heat shrink tubing and confined on both end planes by a steel plug. The assembly was subsequently stored in a water bath at a constant temperature of 70 ± 2 °C. The electrical conductivity of the assembly was discontinuously measured by impedance spectroscopy and the pore fluid was sampled at the end of the experiment using Ar gas pressure. The experiment is labeled b-Fl-17 in Table 2.

(iv) The flow-through experiments with QLM sandwich samples were conducted by means of a high pressure and temperature permeameter [*Milsch et al.*, 2008]. Confining pressures p_c ranged between 5 and 10 MPa and pore pressures p_p ranged between 2.5 and 5 MPa. Temperatures were varied between 40 and 150 °C. The experiments are labeled ft-s-3 and ft-s-4 in Table 2.

(v) The flow-through experiments with intact rock samples were performed by means of the same apparatus as described above. One Fontainebleau and three Flechtinger sandstone samples were investigated. Confining and pore pressures were 10 and 5 MPa, respectively. Temperatures varied between 30 and 164 °C. H_2O was the starting fluid in the majority of the experiments. In one experiment (ft-Fl-12) a 43.2 mmol/L $NaCl_{aq}$

solution with $\sigma_f(T_0) \approx 477$ mS/m was flushed into a Flechtinger sandstone sample at 70 °C. The experiments are labeled ft-Fo-6, ft-Fl-8, ft-Fl-9, and ft-Fl-12 in Table 2.

Flow prevailed at irregular intervals during the flow-through experiments, i.e., during fluid sampling and during flushing the samples with fresh upstream fluid, depending on the experimental strategy. The pore fluid volume in the porous samples was completely replaced by fluid from the upstream pump during flow episodes which yielded situations of chemical disequilibrium between the solid and the fluid phases. Stagnant phases were typically much longer than the flow phases, i.e., the fluid-mineral system was undisturbed during the longest period of an experiment. During the undisturbed (stagnant) phases of the experiments, the fluid-solid-systems reacted to approach a chemical equilibrium by means of dissolution–precipitation reactions [*Schepers and Milsch*, 2013]. Heating and cooling of the samples was performed in stages to deliberately induce disequilibrium conditions in the fluid-solid-systems. Two scenarios were envisaged during the heating and cooling procedures depending on the experimental strategy of each experiment: flushing the samples at the beginning of each temperature stage with a fluid of a known composition (i.e., deionized H_2O) to investigate the temperature-dependence of the electrical conductivity of the fluid-solid-systems; and heating and cooling without replacing the pore fluid to deliberately induce disequilibrium conditions in the fluid-solid-systems. The temperature intervals during heating or cooling stages ranged between 20 and 30 °C. The heating or cooling procedure was performed at 20 °C/h. The duration until the temperature was equilibrated at each constant temperature stage was about 2 h.

2.3. Sampling of Fluids

Four different methods were applied for the sampling of fluids from the batch and flow-through experiments. Fluid samples were taken with a pipette from the PTFE autoclaves after these were cooled to approximately 50 °C (Type I in Figure 1; b-QLM-3, b-QLM-4, b-QLM-5, and b-Fl-15). A dip tube with a metering valve was used to sample the fluid from the BR-300 autoclave at 5 MPa Ar pressure (Type II in Figure 1; b-Fl-16). At the end of the batch experiments with the H_2O-saturated cylindrical Flechtinger sandstone sample (Type III in Figure 1; b-Fl-17) the pore fluid was squeezed out by Ar gas pressure. The flow-rate of the pore fluid was controlled by manually adjusting the Ar gas pressure on the upstream side of the sample. The fluid sample was collected on the downstream side of the sample by means of a tube that was open to the atmosphere. The sampling of pore fluids from the flow-through experiments (Type IV and V in Figure 1; ft-s-3, ft-s-4, ft-Fo-6, ft-Fl-9) required a pressure relief valve on the downstream side of the porous samples and a valve disconnecting the downstream pump. The upstream pump was operated in constant flow mode (flow rate less than 0.5 mL/min) to prevent turbulence in the sample and the connecting tubes. The pressure relief valve was set to the respective pore pressure of the experiments (2.5 and 5 MPa) to prevent pore pressure changes. Due to the low flow-rate the fluids cooled in the body of the pressure relief valve below boiling temperature. Fluids were irregularly sampled by discrete volumes. The cumulatively sampled volume was larger than the sum of the dead volume on the downstream side of the porous samples plus the pore volume. Thus, the first fluid samples represented this dead volume whereas the last fluid samples resulted from the upstream pump. Mixing of the pore fluid with

the up- and downstream dead volume was limited due to the small inner diameter of the connecting tubes.

3. Analytical Methods

3.1. Analyses of the Fluids

The fluid samples were analyzed with respect to σ_f and c_i. Due to limitations by the volume of sampled fluid aliquots, only one fluid sample was additionally analyzed with respect to pH. The electrical conductivity of the fluids was measured with a WTW TetraCon 325 conductivity probe connected to a WTW LF 325 conductivity meter making use of a linear temperature correction with a temperature correction coefficient $\alpha_f = 0.02\ ^\circ\mathrm{C}^{-1}$ (Equation 4). The temperature dependence of σ_f arises from the influence of temperature on the viscosity of a fluid and thus on the ions' drift speeds in the fluid [e.g., *Revil et al.*, 1998; *Hayashi*, 2004]:

$$\sigma_f(T) = \sigma_f(T_0)\,[1 + \alpha_f\,(T - T_0)]. \tag{4}$$

The reference temperature is $T_0 = 25\ ^\circ\mathrm{C}$. Different values of α_f are given in the literature ranging from 0.0175 to $0.025\ ^\circ\mathrm{C}^{-1}$ for various water compositions [*Hayashi*, 2004]. A value describing experimental data well is $\alpha_f \approx 0.023\ ^\circ\mathrm{C}^{-1}$ [*Revil et al.*, 1998]. This value was used for the calculation of $\sigma_f(T)$ for in situ temperatures. During the batch experiments, measurements were performed at approximately 50 °C. For this purpose, the experiments were quenched by cooling the autoclaves rapidly below boiling temperature. After the measurements the PTFE autoclaves were quickly heated to the same temperature as before quenching.

Cation and anion analyses were performed on fluid aliquots. The aliquots (1 to 2 mL) were diluted with 7.5 mL H_2O and acidified with 0.5 mL concentrated HNO_3 (65 %) resulting in a pH of the solutions below 1. Permanently clear fluid samples were thus obtained. The samples were analyzed with inductively coupled plasma–optical emission spectroscopy (ICP-OES) using a Varian Vista MPX with a radial geometry of the spectrometer with respect to the Ar plasma. Calibration of the ICP-OES was performed with ultra-pure solutions containing Na, Al, Si, K, Ca, and in one case Fe and Ni. The analyzed wavelengths were 589.592, 396.152, 251.611, 769.897, 396.847, 238.204, and 231.604 nm for Na, Al, Si, K, Ca, Fe, and Ni, respectively. On one Flechtinger sandstone pore fluid sample with a comparatively large volume (b-Fl-17), anions were analyzed with a Dionex Dx-120 ion chromatograph. The as sampled fluid was used for the anion analysis. The Dx-120 was equipped with IonPac AG9-HC and AS9-HC anion exchange columns. An aqueous solution of Na_2CO_3 with a concentration of 9×10^{-3} mol/L was used as the eluent. At the end of this experiment, pH was measured on a fluid aliquot with a WTW SenTix 81 pH glass electrode in combination with a WTW Multi 340i device.

3.2. Analyses of the Solid Materials

The mineralogical and chemical compositions of the solid samples were determined by X-ray powder diffraction (XRD) and X-ray fluorescence (XRF). For XRD analyses, a Siemens D5000 and a STOE STADIP diffractometer were used operating with Cu-K_α radiation. Analyses were performed on 1 to 3 g powdered material with a grain size smaller than 30 μm. Crystalline phases were qualitatively and quantitatively analyzed using the GSAS software package for Rietveld refinements [*Larson and Von Dreele*, 2000]

with the graphical user interface EXPGUI [*Toby*, 2001]. XRF analyses were performed with a PANalytical Axios^{mAX} – Advanced operating with a Rh anode.

3.3. Electrical Conductivity of the Porous Samples

In one batch experiment (b-Fl-17) σ_r was determined from impedance spectroscopic measurements on a Flechtinger sandstone sample. The frequency dependent impedance Z (in Ω) and the phase angle γ (in rad) of the assembly were measured at irregular intervals in a two-electrode arrangement by means of a Zahner Zennium Electrochemical Workstation impedance spectrometer. Measurements were performed as a function of the frequency of a sinusoidal AC signal ranging from 1 to 10^3 Hz (Figure 2). Scanning in this frequency range was performed in a loop with 47 steps and a start and end value of 10^3 Hz. The assembly was taken out of the water bath for the measurements. Measurements were made after carefully drying the assembly on the outside to prevent leakage currents along the jacket or the isolated thread rods. With the assumption of negligible impedance of the steel plugs compared to the Flechtinger sandstone sample the electrical conductivity of the sample was:

$$\sigma_r = \frac{L}{\cos\gamma\, Z\, A}, \tag{5}$$

where A is the cross sectional area of the sample and L is the sample length. The impedance is expressed as a complex number with a real and an imaginary part. From the real part of the impedance the ohmic resistance R is calculated by $R = \cos\gamma\, Z$. In the AC frequency range examined in this study the ratio of the ohmic resistance R to the impedance Z was close to 1 due to small phase angles (Figure 2). Thus, the imaginary part of the impedance could be neglected and the AC circuit could be treated as a DC

circuit in which Ohm's law applies. Consequently, the electrical conductivity of the rock sample was determined using the ohmic resistance:

$$\sigma_r = \frac{L}{R\,A}. \tag{6}$$

In the flow-through experiments σ_r was measured in the high pressure and temperature permeameters [*Milsch et al.*, 2008]. The σ_r measurements were performed in a four-electrode arrangement with a variable shunt-resistor making use of Ohm's law. The voltage was imposed with an Agilent 33220A function generator set to produce a 1 V AC sinus peak-to-peak signal with a frequency of 13 Hz. Although the measurements were carried out with an impressed AC signal, applicability of Ohm's law was assumed at this low frequency.

Relative errors of the σ_r measurements amount to approximately 4 to 8 %. Relative errors were calculated by an error propagation of relative errors of the voltage measurements and the length measurements involved in determining σ_r. The width of the potential electrode is approximately 1 mm and thus contributes significantly to the uncertainty of σ_r measurements resulting in relative errors as high as 8 % [*Milsch et al.*, 2008]. However, since errors in length measurements are assumed to be fairly constant throughout a single experiment, measured relative changes of σ_r in the course of a single experiment were exact to a much higher extent.

4. Results

4.1. Electrical Conductivity

4.1.1. Batch Experiments

The electrical conductivity of bulk fluids in contact with Flechtinger sandstone samples increased with time at 70 and 150 °C in batch experiments b-Fl-15 and b-Fl-16 (Figure 3). During the first 20 d at 70 °C, $\sigma_f(T_0)$ increased with time at decreasing rates. Further heating to 150 °C led to a further increase of $\sigma_f(T_0)$. From a runtime of 35 d to the end of the experiments, $\sigma_f(T_0)$ was not correlated to temperature any more: $\sigma_f(T_0)$ increased during the third 70 °C stage and decreased during the third 150 °C stage of experiment b-Fl-15. The maximum $\sigma_f(T_0)$ of the bulk fluids attained in the experiments was ≈ 25 mS/m. The different pressures applied in the experiments ($p_{\max} \approx 0.45$ MPa and $p = 5$ MPa) and the different fluid/solid mass ratios (5.4 and 3.6) did not significantly influence the evolution of $\sigma_f(T_0)$.

The electrical conductivity of an H_2O-saturated Flechtinger sandstone sample increased time-dependently in a batch experiment at 70 °C constant temperature (b-Fl-17, Figure 4). After an initial increase from approximately 9 to 22 mS/m during the first 3 d, σ_r slowly increased to approximately 25 mS/m in the remainder of the experiment. The electrical conductivity of a pore fluid sample taken at the end of the experiment was $\sigma_f(T_0) = 477$ mS/m. The fluid/solid mass ratio in the experiment was 19.57 g/468.94 g $\approx$ 0.04.

Interface phenomena like polarization, capacitance, and inductance had negligible effects on σ_r measurements with this sample, as indicated by a ratio of ohmic resistance over complex impedance, R/Z, close to unity (Figure 2). There was neither a temperature nor a time dependence in R/Z. At the starting conditions with H_2O as the pore fluid and 20 °C, R/Z was similar as after a run duration of 3 d at 70 °C. Furthermore, the change of R/Z with AC frequency was not affected by the run duration.

4.1.2. Flow-through Experiments

The flow-through experiments yielded four general observations of the σ_r evolution (Figure 5):

(i) Temperature changes affected σ_r instantaneously. The temperature dependence of σ_r results from the combined responses of σ_f (Equation 4) and σ_s to temperature changes [*Revil et al.*, 1998].

(ii) Flushing the samples with H_2O led to a reset of σ_r values to temperature-dependent base levels. During flow phases, the samples were flushed with several pore volumes of H_2O ($\sigma_f(T_0) \approx 2.5$ mS/m). Temperature-dependent σ_r base levels of a Flechtinger sandstone sample (ft-Fl-8) were approximately 7.3, 12.3, 22.3, and 36.7 mS/m at 30, 51, 90, and 164 °C, respectively (Figure 5a). At 70 °C, the σ_r base level of another Flechtinger sandstone sample (ft-Fl-9) was approximately 16.9 mS/m (Figure 5b). In a QLM sandwich experiment (ft-s-3) the σ_r base level at 70 °C was 0.05 mS/m (Figure 5c). The base level in the QLM sandwich experiment was approached after a short excursion of σ_r to higher values (≈ 0.6 mS/m) when flow of H_2O through the sandwich sample was initiated.

(iii) The electrical conductivity of porous samples increased with time at decreasing rates at constant temperature and pressure and approached a temperature-dependent steady state. During the first 70 °C phase of a Flechtinger sandstone experiment (ft-Fl-9), σ_r increased from 16.6 to 34.5 mS/m (Figure 5b). In the following 150 °C phase, a further increase from 73.1 to 76.3 mS/m was measured. The cooling to 70 °C resulted in a σ_r decrease to 38.1 mS/m. The difference between σ_r values of the first and the second 70 °C stage before and after the 150 °C phase ($\Delta\sigma_r = 3.6$ mS/m) is in the same range as the increase during the 150 °C phase ($\Delta\sigma_r = 3.2$ mS/m). The increase of σ_r during

the 70 °C stage after flushing the sample with H_2O during fluid sampling at 50 days was comparatively low. The increase of σ_r, here, was only about 0.8 mS/m in 11 d. The increase of σ_r during the following (second) 150 °C stage was approximately 3.5 mS/m in about 7 days.

An experiment with a QLM sandwich (ft-s-3) yielded a slow σ_r increase from 0.08 to 0.19 mS/m during the first 70 °C phase (Figure 5c). During the following 150 °C stage, a further increase from approximately 1 to a maximum value of 1.7 mS/m was observed. However, the σ_r data during the 150 °C period showed substantial noise.

(iv) The electrical conductivity of porous samples approached a constant value during the second 70 °C phase after the samples have been held at 150 °C (Figure 5). A Flechtinger sandstone experiment (ft-Fl-9) yielded a slow decrease of σ_r from 38.1 to 37.2 mS/m in the course of the second 70 °C period (Figure 5b). A QLM sandwich experiment (ft-s-3) showed a slow decrease of σ_r from 0.33 to 0.31 mS/m followed by an abrupt decrease to 0.21 mS/m during the second 70 °C phase (Figure 5c).

4.2. Fluid Chemistry

4.2.1. Batch Experiments

The concentrations of dissolved cations of bulk fluids in contact with the QLM granular aggregates yielded the following mean values and standard deviations from the mean: $c_{Na} = 2.3 \pm 0.8$, $c_{Al} = 0.06 \pm 0.04$, $c_{Si} = 2.5 \pm 1$, $c_K = 0.12 \pm 0.06$, and $c_{Ca} = 0.18 \pm 0.09$ mmol/L (b-QLM-3, b-QLM-4, b-QLM-5; see Table 4 for details).

The trends of c_i (with i = Na, Al, Si, K, Ca) of the bulk fluid in contact with a Flechtinger sandstone sample (b-Fl-16) were variable (Figure 6). The relationship between c_i and temperature was complicated. Upon heating from 70 to 150 °C at approximately

24 d run duration, Na, Al, Si, and K values increased, whereas Ca values decreased. A similar behavior, yet less pronounced, can be observed during the second heating event from 70 to 150 °C at approximately 56 d. After a first increase of c_{Al} due to heating, a decreasing trend can be observed from a run duration of approximately 27 d to 42 d. The concentration of Al was below the detection limit of the ICP-OES during the second heating from 70 to 150 °C at 56 d (therefore the data points are not linked in Figure 6). Again, the two remaining data points for c_{Al} during the second cooling from 150 to 70 °C show a decreasing trend.

The concentrations of dissolved cations measured at the end of another Flechtinger sandstone batch experiment (b-Fl-15) were in agreement with the former observations. A comparison of both experiments shows that c_i was independent of different p-T-histories and fluid/solid mass ratios in this case. Apart from different experimental conditions (pressures were about 0.45 and 5 MPa, the durations of constant temperature phases were different, and the fluid/solid mass ratios were 5.4 and 3.6) the data resulting from the experiment at low pressure (b-Fl-15) confirmed the data resulting from the experiment at higher pressure (b-Fl-16).

The evolved pore fluid of the Flechtinger sandstone sample held at 70 °C in the water bath (b-Fl-17) yielded $c_{\mathrm{Na}} = 3.57$, $c_{\mathrm{Al}} = 0.001$, $c_{\mathrm{Si}} = 0.412$, $c_{\mathrm{K}} = 18.9$, and $c_{\mathrm{Ca}} = 8.28$ mmol/L. The concentrations of anions in the fluid sample were $\mathrm{F}^- = 0.016$, $\mathrm{Cl}^- = 40.5$, and $\mathrm{SO}_4^{2-} = 0.312$ mmol/L. The pH at room temperature was 7.47.

4.2.2. Flow-through Experiments

The Fontainebleau sandstone experiment (ft-Fo-6) showed maxima of the concentrations of Ca, Si, and Fe at the smallest cumulatively sampled volume, which is due to the

relatively large volume of the first fluid sample (Figure 7). The overall low concentrations of Fe and Ni in the upstream fluid of the Fontainebleau sandstone experiment ft-Fo-6 (less than 0.025 mmol/L at 23 mL cumulative volume) showed that corrosion of the wetted stainless steel parts of the permeameter had a negligible effect on the fluid composition (Figure 7). The Na concentration at 23 mL cumulative volume was approximately the same as the concentration in the pore fluid at 3.5 mL cumulative volume. Due to the fact that Na is an abundant element, this behavior of the Na concentration points towards a contamination of the pore fluid system with Na.

The reactions of H_2O with the Fontainebleau sandstone core led to high concentrations of Si in the pore fluid. The Si concentrations were above the solubility of quartz at 160 °C indicating that amorphous silica cements were dissolved during the stagnant phase of the experiment. The residence time of the fluid at stagnant conditions was approximately 7 d with a temperature history of approximately 4 and 3 d at 162 and 79 °C, respectively. The fluid samples were taken at the end of the experiment at 70 °C. The Si concentration was high in the first fluid sample and decreased with cumulatively sampled volume. Ca and Fe showed similar trends as Si indicating that the measured concentrations resulted mainly from dissolution of the rock sample although Ca and Fe were only present in small amounts in the rock sample (Table 3). Al and K displayed a similar behavior as Si, Ca, and Fe but with smaller concentrations below 0.02 mmol/L (not shown in Figure 7).

Plots of c_i as functions of cumulatively sampled pore fluid volumes from the other flow-through experiments (ft-s-4 and ft-Fl-9) typically showed bell shaped curves with maxima approximating the pore fluid composition (Figure 8). The mixing with up- and downstream fluid (H_2O) was constrained to approximately 4 mL cumulative volume.

The fluid sample from the QLM sandwich experiment (ft-s-4) yielded $c_{\mathrm{Na}} = 2.2$, $c_{\mathrm{Al}} = 0.0054$, $c_{\mathrm{Si}} = 7.07$, $c_{\mathrm{K}} = 0.099$, and $c_{\mathrm{Ca}} = 1.511$ mmol/L (see Table 4). The residence time of the fluid in the pore space at stagnant conditions was about 16 d with a temperature history of approximately 14 and 2 d at 150 and 70 °C, respectively. The fluid samples were taken during the experiment at a run duration of approximately 30 d at 70 °C.

The dissolution of rock constituents of a Flechtinger sandstone core sample (ft-Fl-9) yielded relatively high concentrations of Na, Si, K, and Ca in the pore fluid compared to c_i of the QLM sandwich experiment (Figure 8). The residence time of the fluid in the pore space at stagnant conditions was about 48 d with a temperature history of approximately 22, 3, 14, 4, and 5 d at 70, 150, 70, 42, and 70 °C, respectively. The fluid samples were taken after a run duration of approximately 50 d at 70 °C.

5. Discussion

5.1. Electrical Rock Conductivity as an Indicator for Dissolution-Precipitation Reactions

The time-dependent changes of σ_r during stagnant phases of the flow-through experiments reflected time-dependent changes of σ_f of the pore fluid. This interpretation is supported by the following observations:

(i) The flow-through experiments with Flechtinger sandstone samples and a QLM sandwich sample showed a time-dependent increase of σ_r at stagnant conditions of the pore fluid and at constant temperature and pressure (Figure 5). The decreasing rate of the σ_r increase can be explained by a decreasing driving force for the dissolution of minerals as c_i increases. This is coherent with published results of batch experiments with Soxhlet-extracted and as received clay- and carbonate-bearing Pictured Cliffs sandstone

samples in contact with tap water as the starting fluid at approximately 25 °C [*Piwinskii and Weed*, 1976]. Their experiments showed that the rate of increase of σ_r with time was larger in the as received material compared to the Soxhlet-extracted material from which relatively easily soluble minerals were removed before the experiment. In their study, steady state conditions of σ_r and σ_f were reached after approximately 187 d. A three step process was suggested for the observed fluid-rock interactions: Inward diffusion of tap water through the pore structure of the rock, dissolution and outward diffusion of water-soluble material lining the pores of the rock, and clay-water exchange. Clay-water exchange was concluded to have been the dominant factor for the increase of σ_f after approximately 1 d run duration of the experiments.

(ii) Flushing the porous samples with several pore volumes of H_2O led to a reset of σ_r to temperature-dependent base levels (Figure 5). Thus, the evolution of σ_r was related to the chemical evolution of the fluid-solid systems at stagnant conditions. The chemical data suggest that the relative contribution of σ_s to σ_r (Equation 3) did not affect the time-dependent σ_r changes (Table 4). The mobility of hydrated counter cations and protons adsorbed to the mineral surface in the Stern layer governs σ_s and the sites for adsorption on the silica and aluminosilicate mineral surfaces are already occupied at very low c_i. In the case of shaly sands saturated with a NaCl-bearing pore fluid at $T = 25$ °C, σ_s is independent of concentration, if $c_i > 1$ mmol/L [*Revil et al.*, 1998]. In our experiments, the sum of c_i, with i = Na, Al, Si, K, Ca, was higher than 1 mmol/L in both the fluid samples from a Flechtinger sandstone and a QLM sandwich flow-through experiment ($c_i \approx 25.9$ mmol/L in ft-Fl-9 and 4.4 mmol/L in ft-s-4). Thus, the relative contribution of σ_s to σ_r decreased as c_i and σ_f of the pore fluid increased. It must be noted, however,

that the relationship between the frequency-dependent electrical conductivity of porous solids and the chemistry of the pore fluids is complex and subject of ongoing investigations [e.g., *Revil and Florsch*, 2010; *Revil and Skold*, 2011; *Vaudelet et al.*, 2011a, b; *Weller and Slater*, 2012].

(iii) The excursion of σ_r at the end of the QLM sandwich experiment (ft-s-3, Figure 5c) was related to an elektrokinetic process (i.e., the streaming potential) that arose from charge accumulations caused by the flow of counter-charges inside the pore space [*Delgado et al.*, 2007]. The replacement of the evolved pore fluid by H_2O finally led to a decrease of σ_r to initial values. A similar but shorter excursion occurred in the Flechtinger sandstone flow-through experiment ft-Fl-9 when the pore fluid was sampled (at 50 d). The excursion was too short to be displayed in Figure 5b. It lasted only a few minutes due to higher flow rates in experiment ft-Fl-9 compared to experiment ft-s-3.

(iv) A combined interpretation of a Flechtinger sandstone batch experiment (b-Fl-17) and two flow-through experiments (ft-Fl-9 and ft-Fl-12) yielded constraints for the steady state σ_f value of the pore fluid that was approached at 70 °C. The electrical conductivity of a Flechtinger sandstone sample increased time-dependently in batch experiment b-Fl-17 at a constant temperature of 70 °C (Figure 4). The pore fluid recovered from this sample yielded $\sigma_f(T_0) = 477$ mS/m corresponding to $\sigma_f(T) = 971$ mS/m (Equation 4). An aqueous NaCl solution with the same σ_f as this pore fluid sample (with 43.2 mmol/L NaCl) was flushed into a Flechtinger sandstone core at 70 °C in a fluid exchange experiment (ft-Fl-12) resulting in a measured σ_r of approximately 37 mS/m. This σ_r-value was almost identical to the value (37.2 mS/m) that σ_r approached at a constant temperature of 70 °C in flow-through experiment ft-Fl-9 (Figure 5b). The observation that a

flushed-in NaCl solution yielded the same σ_r-value as the evolved pore fluid (Table 4) in a Flechtinger sandstone sample suggests that σ_r was not dependent on the specific ionic species in solution. Moreover, this observation indicates that the chemical evolution of the pore fluid at stagnant conditions, and thus also the evolution of σ_f, accounted for the time-dependent changes of σ_r in the experiments. However, there was a difference in σ_r at 70 °C in the batch and the flow-through experiments (25 mS/m in b-Fl-17 vs. 37 mS/m in ft-Fl-9 and ft-Fl-12) although σ_f was identical in all cases. This difference most likely resulted from additional contact resistances in the two-electrode arrangement of the batch experiment compared to the four-electrode arrangement of the flow-through experiment.

5.2. Scenario for Dissolution-Precipitation Reactions

The evolution of $\sigma_f(T_0)$ in Flechtinger sandstone batch experiments exhibited features indicative for the progress of overall dissolution-precipitation reactions (Figure 3). The trend of $\sigma_f(T_0)$ during the first 70 and 150 °C stages obeys an Arrhenius relationship (i.e., the rate of the $\sigma_f(T_0)$ increase was higher at 150 °C than at 70 °C) indicating that the changes in $\sigma_f(T_0)$ were related to kinetically controlled processes. However, subsequent heating and cooling cycles showed no simple kinetic behavior. Studies of various rock-water systems yielded variable time-dependent trends of c_i and intermediate species during overall dissolution-precipitation reactions [*Mueller and Saxena*, 1977; *Busenberg*, 1978; *Lin and Clemency*, 1980; *Lasaga*, 1983]. Thus, the complex response of $\sigma_f(T_0)$ to temperature after the first heating to 150 °C could be indicative of a complex interaction of dissolution and precipitation that changed with time (Figure 3).

The σ_r evolution in the flow-through experiments yielded a qualitatively similar behavior as the discontinuously measured time-dependent evolution of $\sigma_f(T_0)$ during the

first 70 and 150 °C constant temperature stages in the batch experiments (Figure 5b,c vs. Figure 3). The time-dependent changes of σ_r in flow-though experiments with a Flechtinger sandstone and a QLM sandwich sample (ft-Fl-9 and ft-s-3) are consistent with the following scenario: Approach of a steady state of c_i and σ_f during the first 70 °C stage due to dissolution of solids up to saturation of the pore fluid with dissolved species, supersaturation due to heating to 150 °C, and approach of the steady state of c_i and σ_f from supersaturated conditions during the second 70 °C stage due to precipitation of solid phases from the pore fluid.

5.3. Contribution of Minerals with Different Solubilities to Electrical Conductivity

Pure dissolution of quartz and feldspars in QLM sandwich flow-through experiments yielded low values of σ_r compared to the clay-bearing Flechtinger sandstone samples. The QLM sandwich experiment (ft-s-3), in which the minerals were present in the relative mass proportions of the Flechtinger sandstone, showed a maximum σ_r value at 70 °C of 0.21 mS/m (Figure 5c). This value is approximately 180 times lower than the maximum σ_r value at 70 °C (37.2 mS/m) obtained for a Flechtinger sandstone flow-through experiment (ft-Fl-9, Figure 5b). The electrical conductivity of a fluid sample resulting from another QLM sandwich flow-through experiment (ft-s-4), $\sigma_f(T_0) = 49.5$ mS/m, was only lower by a factor of approximately 10 compared to a Flechtinger sandstone pore fluid sample (b-Fl-17) with $\sigma_f(T_0) = 477$ mS/m highlighting the significance of σ_s for σ_r of the clay-bearing Flechtinger sandstone compared to the clay-free QLM material. However, both materials are not directly comparable as to their pore structure, fluid/solid mass ratio, and distribution of minerals. The pore structure of the QLM material resulted from the dense

packing of mineral grains in the sandwich. The consolidated rock sample had a complex pore structure that was due to the diagenetic history of the material. The fluid/solid mass ratio was approximately 10 times higher in the QLM sandwich (≈ 0.5) compared to the rock sample (≈ 0.05). The mineral grains were homogeneously distributed in the QLM sandwich, but the pore walls in the Flechtinger sandstone were lined with illite and cement minerals partly filled the pores and the pore throats yielding a disproportionately large fluid-solid interface of these minerals compared to their low mass proportion in the rock.

Chemical analyses of the fluids resulting from Flechtinger sandstone batch experiments indicated that the evolution of $\sigma_f(T_0)$ of the Flechtinger sandstone pore fluid and the bulk fluids was dependent on the dissolution of sparingly soluble mineral phases, like quartz and feldspars, as well as on the dissolution of phases dissolving more readily, like chlorides and sulfates. The time-dependent changes of c_i of the main constituents of quartz and feldspar (Na, Al, Si, K, Ca) showed that these minerals dissolved in the Flechtinger sandstone batch experiments at $T \leq 150\,^{\circ}\mathrm{C}$ (Figure 6). Additionally, the chemical analysis of the Flechtinger sandstone pore fluid from experiment b-Fl-17 showed that the dissolution of all mineral phases of the rock (not only the main mineral phases) led to the high value of $\sigma_f(T_0) = 477\,\mathrm{mS/m}$. The analysis of anions in this pore fluid sample yielded high Cl^- concentrations ($c_{\mathrm{Cl}} = 40.5\,\mathrm{mmol/L}$). Although chlorides were not found in the Flechtinger sandstone starting material by XRD investigations (Table 1) there probably were small amounts of chlorides in the Flechtinger sandstone starting material, not detectable by the former method, that dissolved time-dependently and thus contributed to the transient increase of σ_f and σ_r. Compared to the Flechtinger sandstone

pore fluid, experiments performed with the main mineral phases (i.e., QLM granular aggregates) yielded significantly lower values of $\sigma_f(T_0) \leq 9.17$ mS/m in the bulk fluids (Table 4). Besides the relatively high Cl^- concentrations the Flechtinger sandstone pore fluid sample showed significantly higher K and Ca concentrations ($c_K \approx 19$ mmol/L and $c_{Ca} \approx 8$ mmol/L) than the fluids resulting from the QLM experiments ($c_K \approx 0.1$ mmol/L and $c_{Ca} \approx 0.2$ mmol/L). This observation underlines the significance of accessory mineral dissolution and a contribution of cation exchange of illite for the pore fluid composition of Flechtinger sandstone samples.

Minerals with different solubilities affected σ_f and thus σ_r during different stages of the experiments. A comparison of the σ_r evolution at 70 °C before and after fluid sampling in a Flechtinger sandstone flow-through experiment shows two phases (Figure 5b). The rate of increase of σ_r with time was smaller after than before fluid sampling although the experimental conditions were identical (H_2O as the pore fluid, $T = 70$ °C). Relatively easy soluble minerals may have been removed by flushing out the pore fluid during fluid sampling leaving behind the sparingly soluble silicates of the bulk rock which led to a smaller rate of increase of σ_r with time after fluid sampling. In case of interactions between the silicates and the pore fluid dissolution-precipitation reactions may have been provoked [*Schepers and Milsch*, 2013]. These reactions possibly changed the mineral surface composition and the pore topography. The effect of these compositional and topographical changes on σ_s is currently not known.

5.4. Relationship Between Electrical Conductivity and Chemical Composition of Fluid Samples

In general, a concurrent chemical analysis of fluid samples from both batch and flow-through experiments was performed. However, in all but one case (b-Fl-17) this was restricted to cation analysis of the relevant species, mainly due to the limited amount of fluid volumes available. The data of chemical analyses are compiled in Table 4 together with measured fluid and rock conductivities, where applicable. The Flechtinger sandstone pore fluid sample (b-Fl-17) mentioned above yielded anion concentrations c_i of $F^- = 0.016$, $Cl^- = 40.5$, and $SO_4^{2-} = 0.312$ mmol/L.

Given a complete set of analytical data a correlation between fluid conductivity at ambient conditions and chemical composition can be established. In general, $\sigma_f(T_0)$ is proportional to the sum of the products of c_i, the degree of dissociation, α_i, the mobility of ions in solution, μ_i, and the valence z_i [*Schön*, 1996]:

$$\sigma_f(T_0) \propto \sum_{i=1}^{n} \alpha_i \, c_i \, z_i \, \mu_i, \tag{7}$$

where n components contribute to $\sigma_f(T_0)$. When multiplying the sum in Equation 7 with elementary charge, e_0, and the Avogadro constant, N_A, one directly obtains the fluid's conductivity from its chemical composition. Due to the lack of data for anionic concentrations this approach can only be evaluated for sample b-Fl-17. However, it is evident from Table 4 that dissolution of matter from the minerals into the fluid has occurred as in all cases both chemical compositions and electrical conductivities depart significantly from the ones of the starting fluid (Section 2.1).

For sample b-Fl-17, the mobilities of the dominant cations and anions in solution at 25 °C are: $\mu_{Na} = 5.19$, $\mu_K = 7.61$, and $\mu_{Ca} = 6.16 \times 10^{-8}$ $m^2 s^{-1} V^{-1}$ [*Revil et al.*, 1998] as well as $\mu_{Cl} = 7.91 \times 10^{-8}$ $m^2 s^{-1} V^{-1}$ [*Weast*, 1984] respectively. From Equation 7 and

Table 4 with $\alpha_i = 1$ one calculates $\sigma_f(T_0) = 564$ mS/m which compares reasonably well to a measured value of $\sigma_f(T_0) = 477$ mS/m. When calculating $\sigma_f(T_0)$ for a 43.2 mmol/L reference NaCl-solution having the same conductivity (Section 5.1) one obtains a value of 546 mS/m, again in reasonable agreement with the measured one.

5.5. Electrical Rock Conductivity as a Proxy for the Kinetics of Dissolution-Reactions

The previous findings imply that changes in rock conductivity are related to kinetically controlled mineral dissolution processes. In the following an exploratory kinetic evaluation will therefore be performed for the conductivity evolution of samples ft-Fl-8 and ft-Fl-9 in Figure 5 up to approximately 39 days at 51 °C and 20 days at 70 °C, respectively. Apart from temperature, both samples reacted under nominally identical conditions. The rock conductivity, here, represents the reaction product B in a reaction A $\rightarrow$ B that can be expressed by a general differential rate law [e.g., *Appelo and Postma*, 1999]:

$$\mathrm{d}/\mathrm{d}t\,[\mathrm{A}] = -k\,[\mathrm{A}]^n, \tag{8}$$

where [A] denotes the concentration of reactant A, k is the rate constant, and n is the reaction order. With $[\mathrm{A}]_0$ the initial concentration of A, then $[\mathrm{A}] = [\mathrm{A}]_0 - [\mathrm{B}]$ and Equation 8 can be expressed as:

$$\mathrm{d}/\mathrm{d}t\,[\mathrm{B}] = k\,([\mathrm{A}]_0 - [\mathrm{B}])^n. \tag{9}$$

Both samples approached some state of equilibrium within the given time intervals. The use of the reaction progress parameter α is therefore appropriate, particularly so because

593 that way the full α-interval between 0 and 1 can be evaluated. For the present case
594 reaction progress can be defined as:

$$\alpha = \frac{\sigma_r(t) - \sigma_r(0)}{\sigma_{\mathrm{r,sat}}(t) - \sigma_r(0)} = [\mathrm{B}]/[\mathrm{A}]_0, \tag{10}$$

595 where $\sigma_r(t)$ is rock conductivity at reaction time t, $\sigma_r(0)$ is rock conductivity at start,
596 and $\sigma_{\mathrm{r,sat}}(t)$ is rock conductivity at saturation or equilibrium, respectively. Equation 10
597 can then be introduced into Equation 9. However, this procedure yields a dependence
598 of the rate constants so derived on both reaction order and initial concentration. In the
599 following, a first order reaction kinetics according to:

$$\alpha = 1 - \exp\left(-k\,t\right), \tag{11}$$

600 will therefore be applied to calculate k as a function of temperature, where t is reaction
601 time. Figure 9 shows reaction progress as a function of time for both samples. Evidently,
602 the rate at which rock conductivity increases becomes higher when temperature is in-
603 creased. Applying Equation 11 to the data in Figure 9 yields $k = 1.36 \times 10^{-6}\ \mathrm{s}^{-1}$ and
604 $2.62 \times 10^{-6}\ \mathrm{s}^{-1}$ for ft-Fl-8 (51 °C) and ft-Fl-9 (70 °C), respectively. The fitted curves in
605 Figure 9 are based on Equation 11 including the respective rate constant and reproduce
606 the original data reasonably well.

607 In a second step the Arrhenius equation can be applied:

$$k = A \exp(-E_a^*/R\,T), \tag{12}$$

where A is a pre-exponential factor, R is the ideal gas constant (8.314 J/mol K), and T is absolute temperature, and E_a^* is the apparent activation energy. From the logarithmic form of Equation 12 E_a^* can be derived. This procedure finally yields $E_a^* = 32$ kJ/mol.

Previous studies on dissolution of minerals of interest for the present study indicated E_a^* values in the range of 60 ± 30 kJ/mol [e.g., *Lasaga*, 1984]. This compares reasonably well to the value derived here. This implies that, in fact, detectable quartz and silicate dissolution has occurred in the course of the experiments. However, from the chemical pore fluid analysis it is evident that additional dissolution of chlorides and sulfates as accessory minerals in Flechtinger sandstone has occurred. A more differentiated analysis on the relative effects of individual dissolution reactions on rock conductivity occurring in a sample at the same time, however, must be left to future investigations.

6. Conclusions

First observations made by *Kristinsdóttir et al.* [2010] indicated that measurements of rock conductivity can probe time-dependent changes in pore fluid chemistry and thus fluid-rock interactions. For evaluating this finding a systematic combination of conductivity measurements and chemical fluid analyses was performed during and after hydrothermal batch and flow-through experiments. The investigations were conducted with quartz-feldspar granular aggregates as well as Fontainebleau and Flechtinger sandstone samples in contact with aqueous solutions.

Overall fluid-mineral reactions, induced by initial disequilibrium conditions, resulted in time-dependent changes in fluid and rock conductivity as well as chemical fluid composition. The batch experiments yielded variable and time-dependent fluid compositions indicating that several individual reactions contributed to the concentrations of dissolved

ions in the bulk fluids. The flow-through experiments showed that the evolution of rock conductivity at constant p-T-conditions was directly related to the evolution of pore fluid conductivity. This finding was supported by a number of evidences: (i) chemical analysis of pore fluid samples indicated a significant increase in cation and anion concentrations compared to the starting fluid, (ii) based on this analysis the measured fluid conductivity was reproduced by calculation within reasonable precision, (iii) when flushing the sample with a reference fluid of known composition and conductivity the rock conductivity was identical to the one measured before sampling the original fluid.

To show the potential of the method an exploratory kinetic evaluation of the data was finally performed to derive an overall apparent activation energy E_a^* of dissolution in Flechtinger sandstone at the present p-T-conditions. E_a^* values were obtained that are comparable to those reported elsewhere for quartz and silicate dissolution. However, chemical pore fluid analysis, here, indicated relatively high chloride concentrations and thus the presence of accessory salt minerals. This finally implies that both the measured evolution of rock conductivity and the calculated apparent activation energy are integrated values over all reactions occurring in parallel within a sample.

It is concluded that electrical conductivity measurements performed at the sample scale can provide high resolution time-resolved monitoring of chemical processes occurring within the pore space of a rock. This, in particular, is true when the conductivity of the background electrolyte is not too high. The method can even deliver quantitative results when appropriate fluid sampling and analyses can be preformed concurrently.

Acknowledgments. The authors would like to thank Tanja Ballerstedt, Ronny Giese, Andreas Kratz, Siegfried Raab, Erik Spangenberg, and the GFZ machine shop staff.

Hans-Peter Nabein, Rudolf Naumann, and Sabine Tonn are acknowledged for substantial analytical support in connection with XRD measurements and ICP-OES. Moreover, the authors wish to thank Sandra Kons for the preparation of some of the starting materials. Fabrice Brunet and one anonymous reviewer are acknowledged for their comprehensive evaluation of the manuscript. This work was financially supported by the Federal Ministry for the Environment, Nature Conservation, and Nuclear Safety under grants BMU 0327682 and BMU 0325069A as well as by the Federal Ministry of Education and Research under grant BMBF 03G0671A.

References

Appelo, C., and D. Postma (1999), *Geochemistry, Groundwater and Pollution*, 536 pp., Balkema.

Archie, G. E. (1942), The electrical resistivity log as an aid in determining some reservoir characteristics, *Transactions of the American Institute of Mining and Metallurgical Engineers*, *146*, 54–62, doi:10.2118/942054-G.

Busenberg, E. (1978), The products of the interaction of feldspars with aqueous solutions at 25 °C, *Geochim Cosmochim Acta*, *42*(11), 1679–1686, doi:10.1016/0016-7037(78)90256-9.

Bussian, A. E. (1983), Electrical conductance in a porous medium, *Geophysics*, *48*(9), 1258–1268, doi:10.1190/1.1441549.

Chelidze, T. L., and Y. Guéguen (1999), Electrical spectroscopy of porous rocks: a review - I.Theoretical models, *Geophys J Int*, *137*, 1–15, doi:10.1046/j.1365-246x.1999.00810.x.

David, C., M. Darot, and D. Jeannette (1993), Pore structures and transport properties of sandstone, *Transport Porous Med*, *11*(2), 161–177, doi:10.1007/BF01059632.

de Lima, O. A. L., and M. M. Sharma (1990), A grain conductivity approach to shaly sandstones, *Geophysics*, *55*(10), 1347–1356, doi:10.1190/1.1442782.

Delgado, A., F. González-Caballero, R. Hunter, L. Koopal, and J. Lyklema (2007), Measurement and interpretation of electrokinetic phenomena, *J Colloid Interf Sci*, *309*(2), 194–224, doi:10.1016/j.jcis.2006.12.075.

Flóvenz, O. G., L. S. Georgsson, and K. Árnason (1985), Resistivity structure of the upper crust in iceland, *J Geophys Res*, *90*(B12), 10,136–10,150, doi:10.1029/JB090iB12p10136.

Glover, P. W., M. J. Hole, and J. Pous (2000), A modified Archie's law for two conducting phases, *Earth Planet Sci Lett*, *180*(3-4), 369–383, doi:10.1016/S0012-821X(00)00168-0.

Glover, P. W. J., P. G. Meredith, P. R. Sammonds, and S. A. F. Murrell (1994), Ionic surface electrical conductivity in sandstone, *J Geophys Res*, *99*(B11), 21,635–21,650, doi:10.1029/94JB01474.

Guéguen, Y., and V. Palciauskas (1994), *Introduction to the physics of rocks*, Princeton University Press, Princeton, New Jersey.

Gunnársson, I., and S. Arnórsson (2000), Amorphous silica solubility and the thermodynamic properties of $H_4SiO_4^0$ in the range of 0 °C to 350 °C at P_{sat}, *Geochim Cosmochim Acta*, *64*(13), 2295–2307, doi:10.1016/S0016-7037(99)00426-3.

Hayashi, M. (2004), Temperature-electrical conductivity relation of water for environmental monitoring and geophysical data inversion, *Environ Monit Assess*, *96*(1), 119–128, doi:10.1023/B:EMAS.0000031719.83065.68.

Hayley, K., L. R. Bentley, M. Gharibi, and M. Nightingale (2007), Low temperature dependence of electrical resistivity: Implications for near surface geophysical monitoring, *Geophys Res Lett*, *34*(18), L18,402–, doi:10.1029/2007GL031124.

Keller, G. V. (1989), *Practical Handbook of Physical Properties of Rocks and Minerals*, chap. Electrical Properties, CRC Press, Boca Raton.

Kristinsdóttir, L. H., O. G. Flóvenz, K. Árnason, D. Bruhn, H. Milsch, E. Spangenberg, and J. Kulenkampff (2010), Electrical conductivity and p-wave velocity in rock samples from high-temperature icelandic geothermal fields, *Geothermics*, *39*(1), 94–105, doi:10.1016/j.geothermics.2009.12.001.

Larson, A. C., and R. B. Von Dreele (2000), General Structure Analysis System (GSAS), Los Alamos National Laboratory Report LAUR 86-748, *Tech. rep.*, Los Alamos National Laboratory.

Lasaga, A. C. (1983), *Kinetics of geochemical processes*, *Reviews in Mineralogy*, vol. 8, Mineralogical Society of America Geochemical Society.

Lasaga, A. C. (1984), Chemical kinetics of water-rock interactions, *J Geophys Res*, *89*(B6), 4009–4025, doi:10.1029/JB089iB06p04009.

Lin, F., and C. Clemency (1980), The kinetics of dissolution of muscovites at 25 °C and 1 atm CO_2 partial pressure, *Third International Symposium on Water-Rock Interaction*, pp. 44–47.

Marshall, W. L. (1980), Amorphous silica solubilities - I. Behavior in aqueous sodium nitrate solutions; 25–300 °C, 0–6 molal, *Geochim Cosmochim Acta*, *44*(7), 907–913, doi:10.1016/0016-7037(80)90280-X.

718 Milsch, H., E. Spangenberg, J. Kulenkampff, and S. Meyhöfer (2008), A new apparatus for
719 long-term petrophysical investigations on geothermal reservoir rocks at simulated in-situ
720 conditions, *Transport Porous Med*, *74*(1), 73–85, doi:10.1007/s11242-007-9186-4.
721 Moore, D. M., and R. C. Reynolds (1989), *X-ray diffraction and the identification and*
722 *analysis of clay minerals*, 332 pp., Oxford University Press.
723 Mueller, R. F., and S. K. Saxena (1977), *Chemical Petrology*, 394 pp., Springer, New-York.
724 Nettelblad, B., B. Ahlen, G. A. Niklasson, and R. M. Holt (1995), Approximate determi-
725 nation of surface conductivity in porous media, *J Phys D Appl Phys*, *28*(10), 2037–2045,
726 doi:10.1088/0022-3727/28/10/007.
727 Pashley, R. M., M. Rzechowicz, L. R. Pashley, and M. J. Francis (2005), De-gassed water
728 is a better cleaning agent, *J Phys Chem B*, *109*(3), 1231–1238, doi:10.1021/jp045975a.
729 Piwinskii, A. J., and H. C. Weed (1976), Study of rock-solution interaction and its effect
730 on Archie's Law, *IEEE Transactions on Geoscience Electronics*, *14*(4), 221–223.
731 Regberg, A., K. Singha, M. Tien, F. Picardal, Q. Zheng, J. Schieber, E. Roden, and S. L.
732 Brantley (2011), Electrical conductivity as an indicator of iron reduction rates in abiotic
733 and biotic systems, *Water Resour Res*, *47*(4), W04,509–, doi:10.1029/2010WR009551.
734 Rein, A., R. Hoffmann, and P. Dietrich (2004), Influence of natural time-dependent varia-
735 tions of electrical conductivity on DC resistivity measurements, *J Hydrol*, *285*, 215–232,
736 doi:10.1016/j.jhydrol.2003.08.015.
737 Revil, A., I. Cathles, L. M., S. Losh, and J. A. Nunn (1998), Electrical conductivity in
738 shaly sands with geophysical applications, *J Geophys Res*, *103*(B10), 23,925–23,936,
739 doi:10.1029/98JB02125.

Revil, A., and N. Florsch (2010), Determination of permeability from spectral induced polarization in granular media, *Geophys J Int*, *181*, 1480–1498, doi:10.1111/j.1365-246X.2010.04573.x.

Revil, A., and P. W. J. Glover (1997), Theory of ionic-surface electrical conduction in porous media, *Phys Rev B*, *55*(3), 1757–1773, doi:10.1103/PhysRevB.55.1757.

Revil, A., and P. W. J. Glover (1998), Nature of surface electrical conductivity in natural sands, sandstones, and clays, *Geophys Res Lett*, *25*, 691–694, doi:10.1029/98GL00296.

Revil, A., D. Hermitte, E. Spangenberg, and J. J. Cochemé (2002), Electrical properties of zeolitized volcaniclastic materials, *J Geophys Res*, *107*(B8), 2168–, doi:10.1029/2001JB000599.

Revil, A., and M. Skold (2011), Salinity dependence of spectral induced polarization in sands and sandstones, *Geophys J Int*, *187*(2), 813–824, doi:10.1111/j.1365-246X.2011.05181.x.

Roberts, J. J., B. P. Bonner, and P. W. Kasameyer (2001), Electrical resistivity measurements of intact and fractured geothermal reservoir rocks, in *Proceedings Twenty-Sixth Workshop on Geothermal Reservoir Engineering*, Stanford University, Stanford, California.

Roberts, J. N., and L. M. Schwartz (1985), Grain consolidation and electrical conductivity in porous media, *Phys Rev B*, *31*(9), 5990–5997, doi:10.1103/PhysRevB.31.5990.

Ruffet, C., M. Darot, and Y. Guéguen (1995), Surface conductivity in rocks: A review, *Surv Geophys*, *16*(1), 83–105, doi:10.1007/BF00682714.

Schepers, A., and H. Milsch (2013), Dissolution–precipitation reactions in hydrothermal experiments with quartz–feldspar aggregates, *Contrib Mineral Petrol*, *165*(1), 83–101,

763 doi:10.1007/s00410-012-0793-x.

764 Schön, J. (1996), *Physical Properties of Rocks - Fundamentals and Principles of Petro-*
765 *physics*, *Handbook of geophysical exploration - seismic exploration*, vol. 18, Pergamon.

766 Sen, P. N., and P. A. Goode (1992), Influence of temperature on electrical conductivity
767 on shaly sands, *Geophysics*, *57*(1), 89–96, doi:10.1190/1.1443191.

768 Sen, P. N., P. A. Goode, and A. Sibbit (1988), Electrical conduction in clay bearing sand-
769 stones at low and high salinities, *J Appl Phys*, *63*(10), 4832–4840, doi:10.1063/1.340476.

770 Toby, B. (2001), EXPGUI, a graphical user interface for GSAS, *J Appl Crystallogr*, *34*,
771 210–213, doi:10.1107/S0021889801002242.

772 Vaudelet, P. A. Revil, M. Schmutz, M. Franceschi, and P. Bégassat (2011), Induced
773 polarization signatures of cations exhibiting differential sorption behaviors in saturated
774 sands, *Water Resour Res*, *47*(2), W02526–, doi:10.1029/2010WR009310.

775 Vaudelet, P. A. Revil, M. Schmutz, M. Franceschi, and P. Bégassat (2011), Changes in
776 induced polarization associated with the sorption of sodium, lead, and zinc on silica
777 sands, *J Colloid Interface Sci*, *360*(2), 739–752, doi:10.1016/j.jcis.2011.04.077.

778 Waxman, M. H., and L. J. M. Smits (1968), Electrical conductivities in oil-bearing shaly
779 sands, *Transactions of the American Institute of Mining, Metallurgical, and Petroleum*
780 *Engineers*, *243*, 107–122, doi:10.2118/1863-A.

781 Weast, R. C. (Ed.) (1984), *CRC Handbook of Chemistry and Physics*, 64th ed., CRC
782 Press, Boca Raton.

783 Weed, H. C., A. J. Piwinskii, and P. R. Keller (1977), Time dependent electrical prop-
784 erties of rock-solution systems, *SPE International Oilfield and Geothermal Chemistry*
785 *Symposium, 27-28 June 1977, San Diego, California*, pp. 213–220.

786 Weller, A., and L. Slater (2012), Salinity dependence of complex conductivity of uncon-
787 solidated and consolidated materials: Comparisons with electrical double layer models,
788 *Geophysics*, *77*(5), D185–D198, doi:10.1190/GEO2012-0030.1.
789 Yang, X., H. Keppler, C. McCammon, H. Ni, Q. Xia, and Q. Fan (2011), Effect of water on
790 the electrical conductivity of lower crustal clinopyroxene, *J Geophys Res*, *116*, B04208,
791 doi:10.1029/2010JB008010.

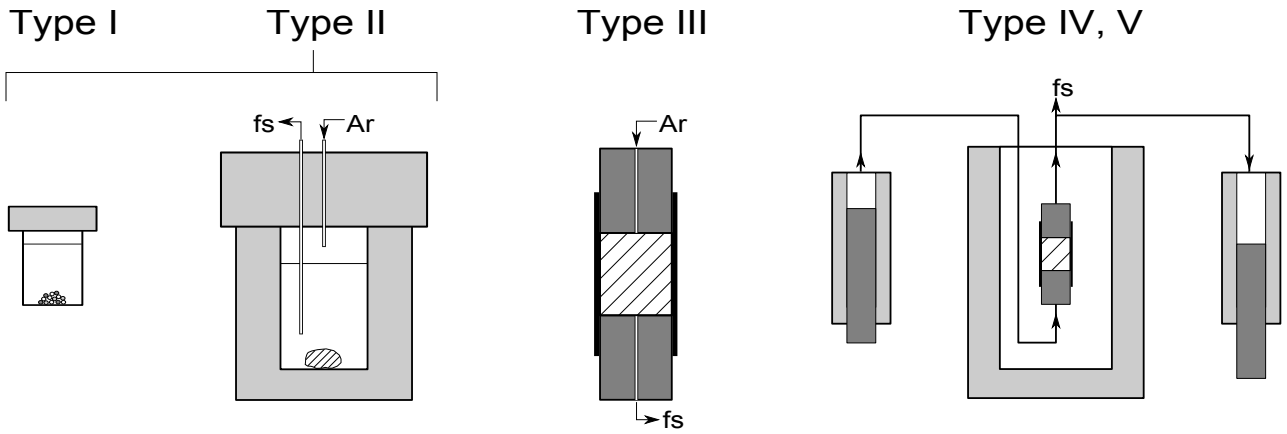

Figure 1. Sketch of the experimental set-ups. Type I are simple batch experiments performed with quartz-feldspar aggregates in PTFE autoclaves. Type II was performed with rock samples using the same autoclave as in Type I as well as a larger Ar-pressurized PTFE lined autoclave. Fluid samples (fs) were taken at irregular intervals while the Ar pressure was held constant. Type III consisted of a sealed rock sample immersed in a water bath. At the end of the experiment a pore fluid sample (fs) was flushed out of the rock sample by means of Ar pressure. In Type IV and V a flow-through apparatus was used to simulate in situ conditions of deep sedimentary reservoirs more closely. The upstream and downstream syringe pumps are shown as well as the pressure vessel containing the sample assembly in the center. The samples in Type IV were granular aggregates of quartz and feldspar. In Type V intact rock samples were investigated. Pore fluid samples (fs) were taken at irregular intervals by means of a pressure relief valve.

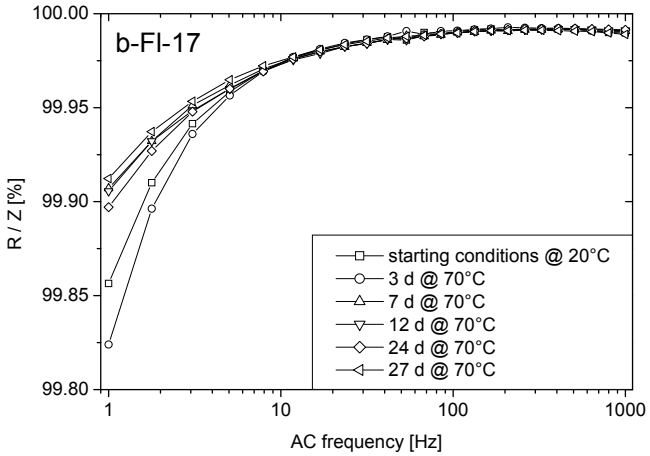

Figure 2. The ratio of ohmic resistance to complex impedance, R/Z, in % as a function of AC frequency in Hz for batch experiment b-Fl-17. R is almost equal to Z in the AC frequency range 1 to 1000 Hz. R/Z is independent of temperature and run duration of the experiment at AC frequencies > 10 Hz. The electrical conductivity of all samples in the flow-through and batch experiments was calculated using R values measured at 13 and 12 Hz, respectively.

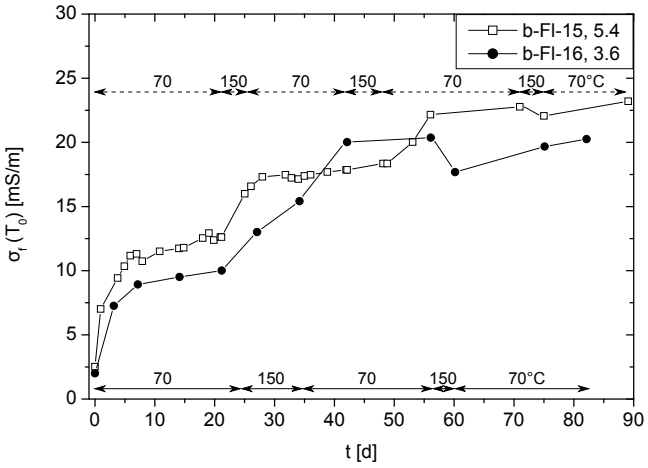

Figure 3. Electrical conductivity of fluids, $\sigma_f(T_0)$, as a function of time for Flechtinger sandstone batch experiments b-Fl-15 and b-Fl-16 at 70 and 150 °C. Fluid/solid mass ratios are given in the legend (5.4 and 3.6, respectively). The temperature histories of experiments b-Fl-15 and b-Fl-16 are illustrated as dashed and solid arrows, respectively. Experiment b-Fl-15 was performed in a 10 mL PTFE batch reactor at a maximum pressure of ≈ 0.45 MPa. Experiment b-Fl-16 was conducted in a 300 mL BR-300 pressurized batch reactor at a constant pressure of 5 MPa. $\sigma_f(T_0)$ shows a similar time-dependent behavior in both experiments, irrespective of the different experimental conditions.

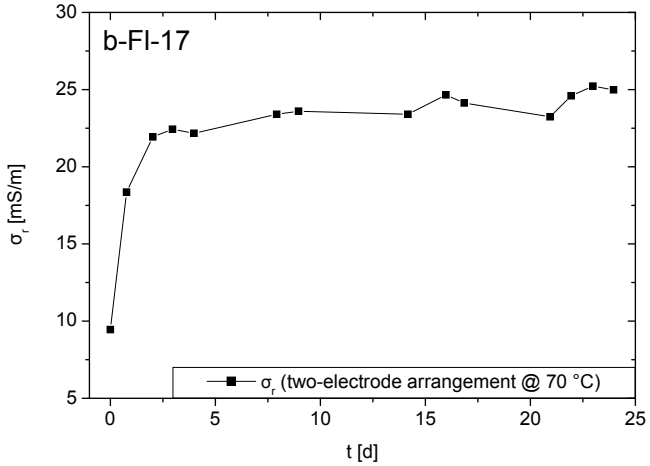

Figure 4. Electrical conductivity, σ_r, of a Flechtinger sandstone sample as a function of time in experiment b-Fl-17 at a constant temperature of 70 ± 2 °C. The data result from impedance measurements performed in a two-electrode arrangement at 12 Hz AC frequency. σ_r shows a time-dependent increase and approaches a steady state value of ≈ 25 mS/m.

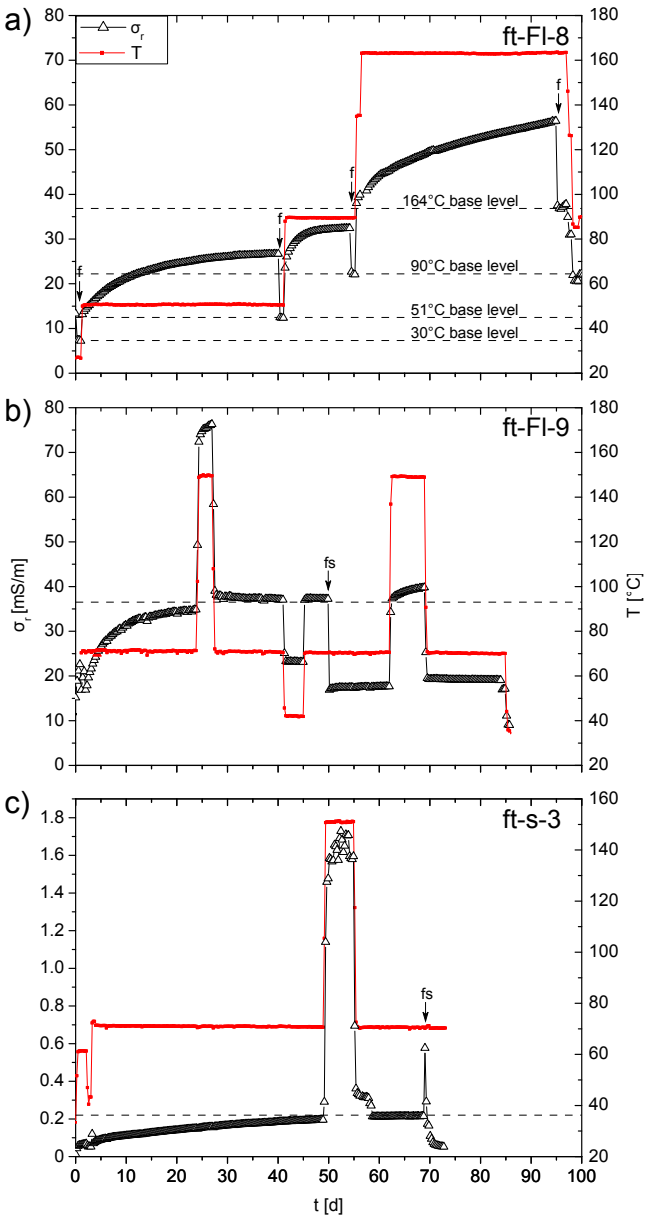

Figure 5. Electrical conductivity of bulk samples, σ_r, and temperature as a function of time for flow-through experiments ft-Fl-8 (a), ft-Fl-9 (b), and ft-s-3 (c). The dashed lines in a) indicate temperature-dependent σ_r base levels. The dashed lines in b) and c) approximate σ_r levels that were approached during 70 °C stages of the experiments. Stagnant conditions prevailed except at the beginning and the end of each constant temperature stage for ft-Fl-8 and at fs-labeled phases in ft-Fl-9 and ft-s-3. f- and fs-labeled arrows denote flow and fluid sampling, respectively. The drop of σ_r to temperature-dependent base levels when the pore fluid was replaced by fresh H_2O shows that the evolution of σ_r was dependent on the evolution of σ_f.

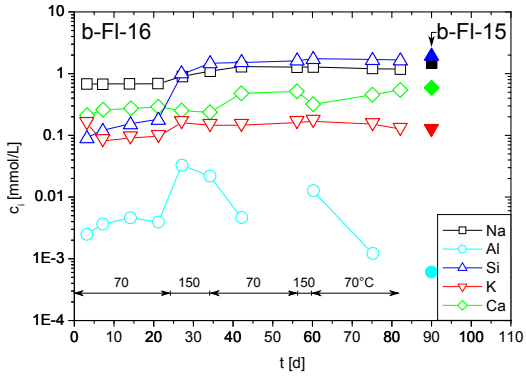

Figure 6. Concentrations of dissolved cations, c_i, as a function of time in batch experiments b-Fl-15 and b-Fl-16. Solid symbols refer to experiment b-Fl-15, open symbols refer to experiment b-Fl-16. Errors of the measurements were on the order of the symbol size. Durations of constant temperature stages in experiment b-Fl-16 are indicated by arrows. The response of the concentrations of Na, Al, Si, K, and Ca to temperature changes was variable. The data for the two experiments are in agreement although the experimental conditions (p-T-history and fluid/solid mass ratio) were different.

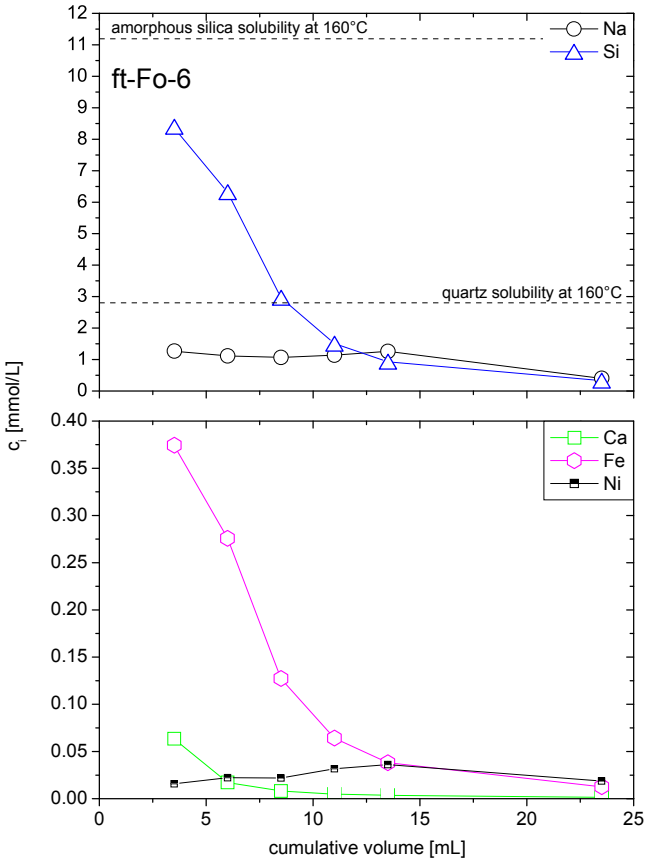

Figure 7. Concentrations of Na, Si, Ca, Fe, and Ni as a function of cumulatively sampled volume from experiment ft-Fo-6. The residence time of the fluid at stagnant conditions was ≈ 7 d with a temperature history of approximately 4 and 3 d at 162 and 79 °C, respectively. Maximum concentrations of the analyzed elements are at 3.5 mL cumulative volume. These concentrations are regarded as an approximation to the pore fluid composition. Errors of the measurements were on the order of the symbol size. The dashed lines represent solubilities of amorphous silica and quartz, respectively, at 160 °C and saturation vapor pressure [*Marshall*, 1980; *Gunnársson and Arnórsson*, 2000]. The concentrations of Si, Fe, and Ca result from dissolution of the Fontainebleau sandstone; the low Ni concentration indicates that corrosion of the wetted parts of the flow-through apparatus used was negligible.

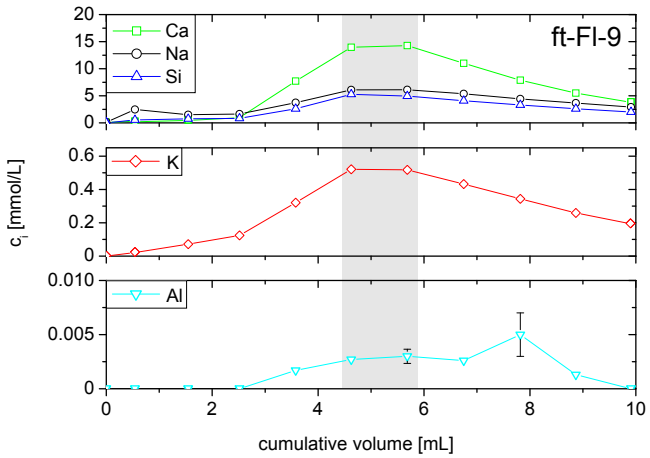

Figure 8. Concentrations of Na, Al, Si, K, and Ca as a function of cumulatively sampled volume from experiment ft-Fl-9. The fluid samples resulted from a Flechtinger sandstone core that was held at different temperature stages for a duration of $\approx$ 50 days with H_2O as the initial pore fluid (Figure 5b). Maximum concentrations of the analyzed elements at approximately 4.5 to 6 mL cumulative volume (the gray shaded area) are regarded as an approximation of the pore fluid composition. Errors were mostly on the order of the symbol size. The data point of the Al concentration at 7.8 mL cumulative volume is assumed to be an outlier value.

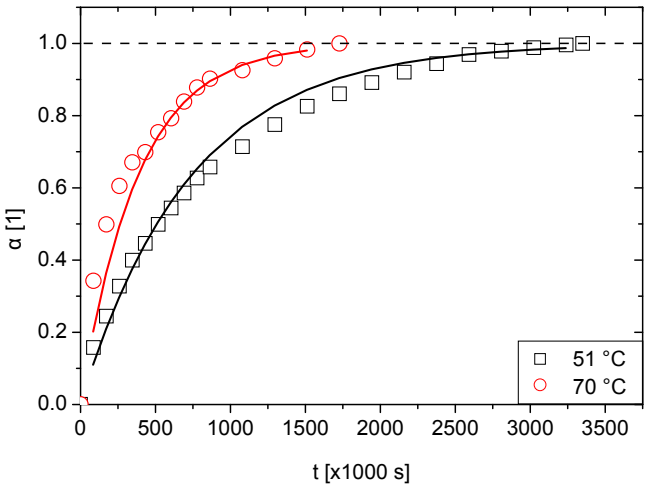

Figure 9. Reaction progress as a function of time for Flechtinger sandstone samples ft-Fl-8 (squares, 51 °C) and ft-Fl-9 (circles, 70 °C). Reaction rate evidently increases with increasing temperature. Bold lines indicate fits to the data based on Equation 11 and the rate constants derived.

Table 1. Starting Materials

Starting material	Petrological description	Chemical composition[a]
quartz	rounded quartz grains from Fontainebleau sandstone	SiO_2
labradorite	pegmatitic crystals from Ihosy, Madagascar	$(Ca_{0.51}Na_{0.42}K_{0.03})Al_{1.49}Si_{2.47}O_8$
microcline with perthitic exsolution lamellae	pegmatitic crystals from Kragerø, Norway	$(K_{0.6}Na_{0.36})Al_{1.01}Si_{2.96}O_8$
Fontainebleau sandstone	quartz arenite	SiO_2
Flechtinger sandstone	$\approx$ 65 % quartz	SiO_2
	$\approx$ 14 % K-feldspar	$KAlSi_3O_8$
	$\approx$ 10 % corroded plagioclase	$Na_{0.5}Ca_{0.5}Al_{1.5}Si_{2.5}O_8$ [b]
	$\approx 7-8$ % illite (pore filling)	$(Ca_{0.05}Na_{0.03}K_{0.61})(Al_{1.53}Fe^{3+}_{0.22}Fe^{2+}_{0.03}Mg_{0.28})(Si_{3.4}Al_{0.6})O_{10}(OH)_2$ [c]
	$\approx$ 3 % calcite cement	$CaCO_3$
	other cements[d]	e.g. Fe_2O_3
	volcanic rock fragments[d]	various
	accessory minerals[d]	e.g. $BaSO_4$, TiO_2

[a] Chemical composition determined by XRD and XRF.

[b] Chemical composition of andesine-labradorite.

[c] Average chemical composition taken from *Moore and Reynolds* [1989].

[d] Present in variable amounts.

Table 2. Overview of the Experiments

Number[a]	Type[b]	Grain size [μm]	Solid mass [g]			Fluid	Fluid mass [g]	T-Range [°C]	p_c [MPa]	p_p [MPa]	Duration [d]
b-QLM-3	QLM series	63-125	1 ± 0.013			H_2O	5	150	≈ 0.45	n.a.	7
b-QLM-4	QLM	63-125	Q: 0.724;	L: 0.115;	M: 0.164	H_2O	5	70-150	≤ 0.45	n.a.	52
b-QLM-5	QLM	63-125	Q: 0.724;	L: 0.118;	M: 0.164	H_2O	5	150	≈ 0.45	n.a.	70
b-Fl-15	Flechtinger SST	n.a.	0.931			H_2O	5	70-150	≤ 0.45	n.a.	90
b-Fl-16	Flechtinger SST	n.a.	66.85			H_2O	240	70-150	5	n.a.	82
b-Fl-17	Flechtinger SST	n.a.	468.94			H_2O	19.57	70	≈ 0.1	n.a.	38
ft-s-3	QLM sandwich with Fontainebleau SST	63-125	Q: 1.447;	L: 0.229;	M: 0.33	H_2O	≈ 2[c]	40-150	10	5	75
ft-s-4	QLM sandwich with porous PTFE	63-125	Q: 1.446;	L: 0.233;	M: 0.328	H_2O	≈ 1[c]	40-150	5	2.5	48
ft-Fo-6	Fontainebleau SST	n.a.	69.29			H_2O	≈ 2[c]	40-162	10	5	40
ft-Fl-8	Flechtinger SST	n.a.	66.33			H_2O	≈ 3.1[c]	30-164	10	5	136
ft-Fl-9	Flechtinger SST	n.a.	66.3			H_2O	≈ 3.1[c]	40-150	10	5	90
ft-Fl-12	Flechtinger SST	n.a.	65.9			$NaCl_{aq}$[d]	≈ 3.2[c]	70	10	5	0.5

[a] b denotes batch experiment; ft denotes flow-through experiment; QLM denote quartz, labradorite, and microcline, respectively.

[b] SST denotes sandstone.

[c] Initial volume of the pore fluid in the flow-through experiments.

[d] 43.2 mmol/L.

p_c, p_p denote confining and pore pressure, respectively; n.a. denotes not applicable.

Table 3. XRF Data of the Quartz, Labradorite, and Microcline Samples

	Quartz / Fontainebleau SST	Labradorite	Microcline
	[%]	[%]	[%]
SiO_2	99.47	54.95	65.66
TiO_2	0.015	0.054	0.01
Al_2O_3	0.06	28.12	18.96
Fe_2O_3	0.02	0.19	0.02
MnO	0	0	0.01
MgO	0.03	0	0.01
CaO	0.02	10.67	0.2
Na_2O	0.04	4.84	4.08
K_2O	0	0.53	10.42
P_2O_5	0	0.037	0.02
H_2O	0.226	0.367	0.3615
CO_2	0.1275	0.1205	0.091
Sum	100.01	99.88	99.84
Ba	0.0035	0.0193	0.004
Cr	0.0018	0.0016	0.0015
Ga	0.0002	0.0023	0.0041
Nb	0.0005	0.0003	<0.0002
Ni	0.0005	0.0007	0.0009
Rb	0.0003	<0.0003	0.1168
Sr	0.0005	0.1025	0.0015
V	<0.0009	<0.0009	<0.0009
Y	0.0006	0.0005	0.0009
Zn	<0.0002	0.0006	0.0003
Zr	0.0026	0.0031	0.0006

Table 4. Comparison of Concentrations of Ions in Solution, c_i, Maximum Electrical Rock Conductivity at 70 °C, $\sigma_{\mathrm{r,max}}(70)$, and Measured Electrical Conductivity of Fluids, $\sigma_f(T_0)$

Experiment	Na [mmol/L]	Al [mmol/L]	Si [mmol/L]	K [mmol/L]	Ca [mmol/L]	$\sigma_{\mathrm{r,max}}(70)$ [mS/m]	$\sigma_f(T_0)$ [mS/m]
b-QLM-3	2.078	0.0436	1.435	0.0826	0.1085	n.a.	7
b-QLM-3	2.247	0.0780	2.325	0.1073	0.1578	n.a.	9.17
b-QLM-3	2.242	0.0343	2.153	0.0961	0.1562	n.a.	8.92
b-QLM-3	2.208	0.0317	2.429	0.0933	0.168	n.a.	9.12
b-QLM-3	2.11	0.0253	2.521	0.0924	0.1911	n.a.	6.02
b-QLM-4	1.262	0.1424	1.859	0.0917	0.0819	n.a.	7.61
b-QLM-5	4.238	0.0352	4.912	0.255	0.38	n.a.	9.12
b-Fl-15	1.434	0.0006	1.99	0.1319	0.587	n.a.	23.2
b-Fl-16	0.679	0.0025	0.092	0.156	0.21	n.a.	7.26
b-Fl-16	0.682	0.0036	0.121	0.0811	0.2584	n.a.	8.93
b-Fl-16	0.682	0.0046	0.155	0.0908	0.2722	n.a.	9.51
b-Fl-16	0.686	0.0039	0.182	0.0967	0.2897	n.a.	10.01
b-Fl-16	0.899	0.033	0.971	0.1605	0.2511	n.a.	13.02
b-Fl-16	1.095	0.0217	1.476	0.1458	0.2358	n.a.	15.42
b-Fl-16	1.306	0.0046	1.514	0.1463	0.4798	n.a.	20.02
b-Fl-16	1.272	0	1.614	0.1612	0.5145	n.a.	20.37
b-Fl-16	1.285	0.0125	1.75	0.169	0.3185	n.a.	17.68
b-Fl-16	1.199	0.0012	1.698	0.1523	0.4541	n.a.	19.67
b-Fl-16	1.186	0	1.665	0.1268	0.5456	n.a.	20.25
b-Fl-17	3.57	0.001	0.412	18.9	8.28	25	477
ft-s-3	2.03	0.025	1.93	0.077	0.307	0.22	n.a.
ft-s-4	2.2	0.0054	7.07	0.099	1.511	n.a.	49.5
ft-Fl-9	6.12	0.003	4.95	0.52	14.3	37.2	477

n.a. denotes not analyzed.